LBNL-44681
Preprint

ERNEST ORLANDO LAWRENCE
BERKELEY NATIONAL LABORATORY

Photofragment Translational Spectroscopy with State-Selective 'Universal Detection': The Ultraviolet Photodissociation of CS_2

W. Sean McGivern, Osman Sorkhabi, Abbas H. Rizvi, Arthur G. Suits, and Simon W. North

Chemical Sciences Division

December 1999

Submitted to
Journal of Chemical Physics

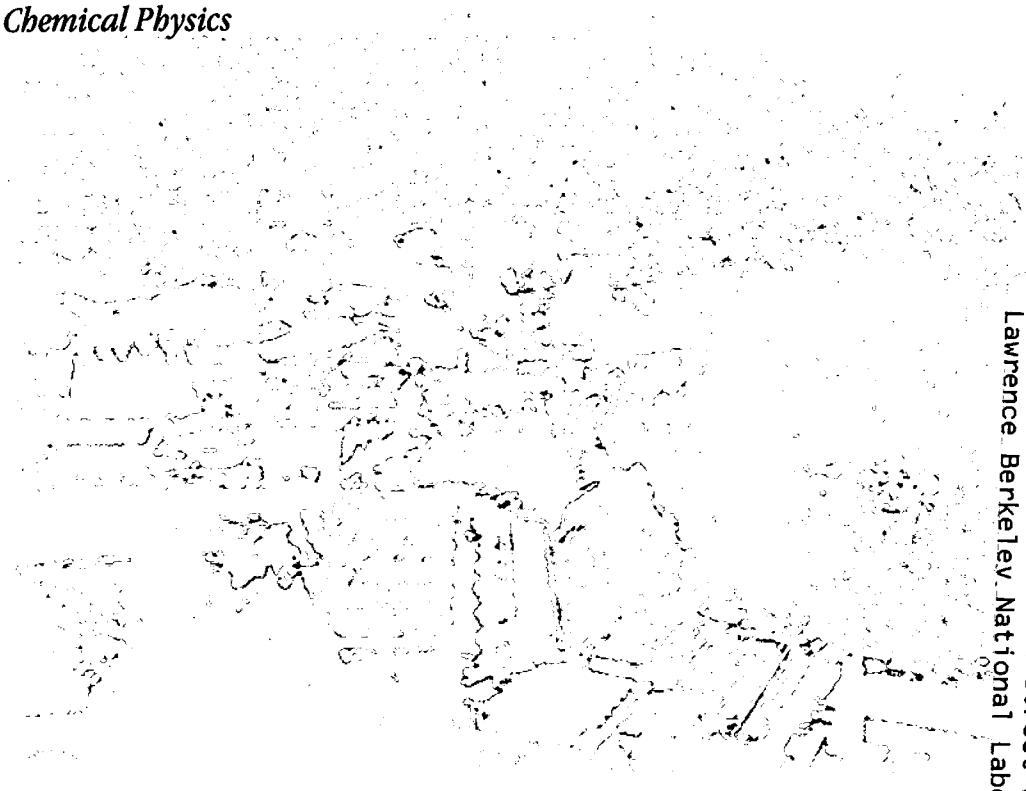

DISCLAIMER

LBNL-44681

Photofragment Translational Spectroscopy with State-Selective 'Universal Detection': The Ultraviolet Photodissociation of CS_2

W. Sean McGivern,[a] Osman Sorkhabi,[b] Abbas H. Rizvi,[b]
Arthur G. Suits,[b] and Simon W. North[a]

[a]Department of Chemistry
Texas A&M University
College Station, Texas 77842

[b]Department of Chemistry
University of California, Berkeley
and
Chemical Sciences Division
Ernest Orlando Lawrence Berkeley National Laboratory
University of California
Berkeley, California 94720

December 1999

This work was supported by the Director, Office of Energy Research, Office of Basic Energy Sciences, Chemical Sciences Division, of the U.S. Department of Energy under Contract No. DE-AC03-76SF00098.

Photofragment Translational Spectroscopy with State-Selective 'Universal Detection' : The Ultraviolet Photodissociation of CS_2

W. Sean McGivern[a], Osman Sorkhabi[b], Abbas H. Rizvi[b], Arthur G. Suits[b] and Simon W. North[a]

[a]*Department of Chemistry, Texas A&M University, College Station TX 77842; and*
[b]*Chemical Sciences Division, Lawrence Berkeley Laboratory, University of California, and Chemistry Department, University of California, Berkeley, CA, 94720*

Abstract

We have investigated the photodissociation of CS_2 at 193 nm using the technique of photofragment translational spectroscopy. The utilization of vacuum ultraviolet synchrotron radiation for product photoionization has permitted a determination of the vibrationally resolved translational energy distribution for the CS + S(^{1}D) channel and the translational energy distribution for the CS + S(^{3}P) channel. A simulation of the coincident S(^{1}D) translational energy distribution is consistent with a CS vibrational distribution of 0.02:0.17:0.19:0.46:0.15 in v=0:1:2:3:4 and an average rotational energy of ~1-3 kcal/mole. We find that the S(^{3}P)/S(^{1}D) branching ratio is 3.0±0.2 in good agreement with previous reports. Both asymptotic channels exhibit similar velocity-dependent anisotropy parameters that decrease with decreasing translational energy release. The results extend earlier reports and provide further insight into the dissociation dynamics at 193 nm.

I. INTRODUCTION

The ultraviolet dissociation of CS_2 has been studied extensively. Excitation near 200 nm results in a transition from the linear $(\pi_g)^4\ ^1\Sigma_g^+$ state to the bent $(\pi_g)^3(\pi_u^*)^1\ ^1\Sigma_u^+$ ($^1B_2$) state.[1,2,3,4,5] The barrier to linearity in the $^1B_2$ state is ~2750 cm^{-1}, corresponding to 49,000 cm^{-1} above the ground state. The $^1B_2$ state is predissociative and results in the following two product channels,

$$CS_2 \rightarrow CS(^1\Sigma^+) + S(^3P_J) \qquad (J = 0,1,2) \qquad [1]$$

$$\rightarrow CS(^1\Sigma^+) + S(^1D_2) \qquad [2]$$

There have been numerous studies of the branching ratio and state distributions of the photodissociation products, the majority of which have focused on dissociation at 193 nm. The determination of the $S(^3P)/S(^1D)$ branching ratio has been a key issue in the dissociation and the subject of conflicting results.[6,7] Waller and Hepburn have established the widely accepted value at 193 nm of 2.8±0.3, favoring the spin-forbidden channel, using vacuum ultraviolet (VUV) laser-induced fluorescence (LIF) of the S atom in a molecular beam.[8] More recently, Hepburn and co-workers have extended their study of CS_2 to wavelengths between 214 and 198 nm. They observe that the atomic branching ratio is highly mode specific below 49,000 cm^{-1} and becomes approximately 2.0 at the shortest wavelengths measured.[4]

There has also been significant work on the CS state distributions and fragment translational energy distributions. The CS fragment is observed in vibrational levels up to v=13 with a maximum near v=3.[9,10,11] The rotational distributions cannot be described by a single temperature and yield an average rotational energy of 1-3 kcal/mol for CS fragments with $v \leq 5$ but significantly higher for $v > 5$.[9,10,12] The product translational energy distribution has been measured using photofragment translational spectroscopy at increasing levels of energy resolution. Neither these experiments, employing electron impact ionization, nor the CS state distributions provide a direct view of the correlated state distributions in the dissociation. Most of these studies, however, have attempted to derive the underlying correlated distributions, often with contradictory results obtained

from very similar experimental data. Early work by Yang *et al.*[12] and Barry *et al.*[13] showed an abrupt break in the translational energy distribution at the onset of the $S(^1D)$ channel, and the authors assigned the low translational energy fragments exclusively to this channel. This analysis resulted in CS ($^1\Sigma^+$) vibrational distributions which were in good agreement with laser induced fluorescence studies but yielded $S(^3P)/S(^1D)$ branching ratios which were less than unity. Later work by Tzeng *et al.*[14] at higher resolution determined individual contributions from channels (1) and (2) by extrapolating the $S(^3P)$ component of the $P(E_T)$ to translational energies below the $S(^1D)$ threshold. The resultant distributions were consistent with the both the $S(^3P)/S(^1D)$ ratio and the coarse translational energy distributions determined by Waller and Hepburn. Impressive signal-to-noise and higher energy resolution characterized the more recent work by Frey and Felder.[15] The experimental data was qualitatively similar to the results of Tzeng *et al.* but included the determination of a translational energy dependence to the anisotropy parameter that had been overlooked in previous studies. Their analysis resulted in a very different partitioning of the total translational energy distribution into the $S(^3P)$ and $S(^1D)$ channel, as well as very different anisotropy parameters for the individual channels.

In the present study we have re-examined the 193 nm photodissociation of CS_2 using photofragment translational spectroscopy combined with VUV ionization and demonstrate the first state-selective ionization and correlated vibrational state distributions measured using this apparatus. The combination of the velocity resolution afforded by neutral time-of-flight methods and state-selective ionization has enabled an unambiguous determination of the $S(^3P)/S(^1D)$ branching ratio, the correlated internal state distributions, and the spatial anisotropy associated with each asymptotic dissociation channel.

II. EXPERIMENTAL

A thorough description of the crossed molecular beam apparatus which uses VUV ionization for product detection has been provided elsewhere.[16] A pulsed supersonic molecular beam was generated by expanding 800 Torr of 9% CS_2 in He through a 0.8 mm nozzle (General Valve Corp.) into a source chamber maintained at $5x10^{-5}$ Torr. The

pulsed valve was heated to 80 °C to inhibit cluster formation. The velocity distribution of the resulting beam was measured by chopping the beam with a slotted mechanical wheel. The beam velocity was 1410 m/s with a full width at half maximum (FWHM) of 12%. The molecular beam was skimmed twice and intersected at 90° with the output of a Lambda Physik LPX-200 excimer laser operating on the ArF transition (193.3 nm). Laser fluences ranged from 10-300 mJ/cm^2. The power dependence of the fragments through this range of fluences indicated that the signal was due to single photon absorption. The molecular beam was rotatable about the axis of the photodissociation laser. Neutral photodissociation products that recoiled out of the molecular beam traveled 15.1 cm where they were intersected by VUV undulator radiation and photoionized, mass selected using a quadrupole mass filter, and counted as a function of time.[17] A pile-of-plates polarizer, consisting of 8 quartz plates at Brewster's angle, was used to polarize the excimer beam, resulting in >85% linear polarization. Rotation of the linear polarized beam was achieved using a half-wave plate (Karl Lambrecht). The VUV undulator radiation used for product photoionization is described in detail elsewhere.[18,19] After passing through the rare gas filter, the undulator radiation is refocussed to 150μm x 250μm at the point of intersection with the scattered neutral photodissociation products. The undulator flux is continuously monitored using a VUV calorimeter.

CS_2, 99+%, was obtained from Aldrich and used without further purification.

III. RESULTS AND DISCUSSION

A. Photofragment Detection at 15 eV

Center-of-mass translational energy distributions, $P(E_T)$, were obtained from the time of flight (TOF) spectra using the forward convolution technique.[20] For all of the TOF spectra presented, the circles represent the data and the solid line is the forward convolution fit. While TOF spectra were taken at multiple laser fluences to ensure that dissociation signals were the result of a single photon absorption, all TOF spectra presented were taken with a laser fluence of 100-400 mJ/cm^2.

The TOF spectra for S atom products (m/e 32) at scattering angles of 10°, 40°, and 60°, obtained using unpolarized light, and a photoionization energy of 15.0 eV are shown

in Figure 1. Earlier studies, employing electron impact ionization detection, observed significant cracking from CS contaminating the m/e 32 spectra and, therefore, only collected signal at m/e 44 (CS^+).[12,13] The TOF spectra were fit with the $P(E_T)$ distribution shown in the top panel of Figure 2. The 15.0 eV ionization energy TOF spectra and the corresponding $P(E_T)$ distributions exhibit vibrational structure, especially in the region where the $S(^1D)$ channel is energetically accessible with a maximum near 8.3 kcal/mol. Vibrational combs corresponding to CS products formed in coincidence with the $S(^3P)$ and $S(^1D)$ channels are indicated above the $P(E_T)$ distribution in Figure 2. The maximum in the $P(E_T)$ distribution corresponds to a CS internal energy consistent with either v=10 for $S(^3P)$ or v=3 for $S(^1D)$. Vaida and co-workers found that expanding CS_2 in Ar or He resulted in spectra that were consistent with a rotationally cold (<10 K) but vibrationally warm (300 K) sample. We expect to achieve more efficient vibrational cooling based on a comparison of expansion conditions and note that even at 300 K, CS_2 will contain less than 1.0 kcal/mol of internal energy on average. There is 45.3 kcal/mol of available energy following $S(^3P)$ atom elimination and 18.9 kcal/mol available for the $S(^1D)$ channel.[21,22] The TOF spectra for m/e 44 (CS^+), the momentum matched partner fragment, at laboratory angles of 30° and 40° and a photoionization energy of 15.0 eV are shown in Figure 3.

The similarity of our derived $P(E_T)$ distribution to those of earlier studies which employed electron impact ionization suggests that photoionization at energies several eV above fragment ionization thresholds provides non-state selective, 'universal' product detection. The momentum matching of the m/e 32 and m/e 44 TOF spectra confirms that at a photon energy of 15.0 eV we observe no selectivity for either sulfur atom electronic state or internal energy state of CS fragment.

TOF signals at m/e 32 and 44 were integrated over ranges of arrival time as a function of polarization angle to determine the anisotropy parameter. The upper plots in Figure 4 show two representative fits to polarized TOF data at m/e 32 and a laboratory angle of 40°. The lower plot of Figure 4 shows the data and fits to two ranges of translational energy; 2.5-7.0 kcal/mol and 20-30 kcal/mol. The anisotropy parameters determined from the fits are indicated on the figure. We find that the anisotropy parameter, β, of the photofragments following correction for the incomplete polarization of the photolysis

beam ranges from β=0.6±0.1 for the highest translational energy fragments (E_T>30 kcal/mol) to 0.1±0.1 at low energies (E_T<5 kcal/mol). We have chosen to fit the data by first measuring polarized TOF spectra at several polarization angles and integrating restricted regions to determine anisotropy parameters corresponding to translational energy ranges. The data was fitted with three separate translational energy distributions, each of which were characterized by a single anisotropy parameter. Several sets of polarized TOF spectra and unpolarized TOF spectra were then fitted by adjusting the relative contributions and shapes of each of these distributions until a satisfactory fit to all the data was achieved. The distributions were then co-added to give the $P(E_T)$ shown in the top panel of Figure 2. No noticeable improvement was obtained by further dividing of the total translational energy distribution.

B. State-selective Detection of $S(^1D)$ at 10.1 eV

Although the total $P(E_T)$ corresponds to the sum of distributions from both asymptotic channels, we were able to isolate the contribution from the $S(^1D)$ channel by recording TOF spectra at photoionization energies below the $S(^3P)$ ionization potential of 10.36 eV.[23] Figure 5 illustrates the difference in the m/e 32 (S^+) TOF spectrum at 40° when the photoionization energy is decreased from 13 eV (top panel) to 10.1 eV (bottom panel). Qualitatively, there is a significant loss of the highest translational energies, corresponding to signal <60 μsec, and a decrease of all the signal relative to the peak at 90 μsec. TOF spectra for m/e 32 recorded at photoionization energies between 10.1 eV and the $S(^1D)$ ionization potential (9.2 eV) did not show measurable differences from the spectra collected at 10.1 eV. We consider this strong evidence that at 10.1 eV only the $S(^1D)$ fragments contribute to the TOF spectra. This marks the first time that state-selected vibrationally-resolved TOF spectra have been reported on this apparatus, demonstrating the viability of measuring correlated distributions in photofragmentation by this technique. The translational energy distribution derived from fitting the 10.1 eV TOF spectra is shown in the bottom panel of Figure 2 (circles) along with the state-averaged, total, $P(E_T)$ (dashed line) for comparison. Determination of the $P(E_T)$ for this channel was based on the analysis of polarized and unpolarized TOF spectra outlined previously. The $S(^1D)$ $P(E_T)$ exhibits more pronounced vibrational structure than the total

$P(E_T)$, particularly an enhancement of the peak consistent with v=3 CS fragments. The lack of vibrational resolution for the $S(^3P)$ channel near threshold is due presumably to the formation all possible J states of the $S(^3P_J)$ atom, which are separated in energy by 187 cm^{-1} between the $^3P_0$ and $^3P_1$ states and 396 cm^{-1} between the $^3P_1$ and $^3P_2$ states.[4] Our derived $S(^1D)$ $P(E_T)$ is in qualitative agreement with the $P(E_T)$ reported by Tzeng, *et al.*[13] and with the vibrationally unresolved LIF measurements of Waller and Hepburn[8], including the location of the maximum at 7 kcal/mol.

The most detailed traditional photofragment translational spectroscopy study prior to this work was performed by Frey and Felder,[15] who obtained correlated translational energy distributions for each channel, which differ significantly from previously reported correlated distributions. The translational energy distribution determined by Frey and Felder for the $S(^1D)$ channel increases quickly from the thermodynamic maximum with decreasing translational energies until showing vibrationally resolved peaks corresponding to v=3. The $S(^3P)$ channel $P(E_T)$ distribution determined by Frey and Felder shows a similar mixture of vibrationally resolved and vibrationally unresolved regions, increasing slowly until the thermodynamic maximum for the $S(^1D)$ channel is reached, where the distribution exhibits strong vibrationally resolved peaks corresponding to v=8 through v=10. The $S(^3P)$ distribution then abruptly decreases to near zero at low translational energies. We find that several features of the Frey and Felder correlated distributions are inconsistent with our results. In particular, we attribute the vibrational structure in the $P(E_T)$ distribution entirely to the $S(^1D)$ channel with no vibrational structure present in the translational energy distribution for the $S(^3P)$ channel.

The $S(^1D)$ translational energy distribution provides considerable information on the coincident CS vibrational and rotational energy distributions. We have simulated the $S(^1D)$ $P(E_T)$ distribution using Gaussian functions in energy to describe the rotational distributions of the individual vibrational states. The final simulation is shown in the lower panel of Figure 2. The solid line in the figure is the total vibrational distribution, and the dashed lines represent the individual contributions from the CS vibrational states. It is interesting to compare the observed correlated CS vibrational distributions to previous LIF results,[8,9,12,13] which measure contributions from CS products that are derived from both the $S(^1D)$ and $S(^3P)$ channels. Our derived distribution for the $S(^1D)$

channel peaks at v=3, in good agreement with the previous LIF studies, although the preference for v=3 in the coincident measurement is more dramatic in the present study. We have determined a coincident vibrational distribution of 0.02:0.17:0.19:0.46:0.15 for v=0:1:2:3:4 CS fragments. Although v=5 CS fragments can energetically be formed in coincidence with S(^{1}D), these products, which have low translational energies, appear at small angles where uncharacterized contributions from cluster dissociation preclude quantification of the v=5 component.

The choice of Gaussian rotational distributions is somewhat arbitrary, though previous studies have found that the distributions were not well described by Boltzmann distributions.[9] We have chosen to use rotational distributions characterized by FWHM of 2.1 kcal/mol. The offsets for the distributions, corresponding to the approximate values of the average rotational energy, are between 1.5-2.5 kcal/mol and are good agreement with previous reports in the literature.[9,12] Jackson and co-workers[24] have found that CS fragments with v≥5 have average rotational energies of ~6 kcal/mol, which are required to be formed in coincidence with S(^{3}P). However, because we cannot select the specific J states of the S(^3P_J) fragments, we cannot resolve CS vibrations formed in coincidence with S(^{3}P) products.

C. Subthreshold Detection of CS Fragments

A dependence of the TOF spectra on photoionization energy due to fragment internal energy has been observed previously.[25,26] Figure 6 shows the m/e 44 (CS^+) TOF spectra at three ionization energies; one above and two below the CS ionization potential of 11.3 eV.[27] The translational energy distributions derived from fitting the m/e 44 TOF spectra are shown in Figure 7 and provide a clearer picture of the origin of the dramatic changes that occur upon lowering the ionization energy. The vibrational structure, well defined in the 12 eV spectrum, is significantly altered at 11eV and is almost completely absent in the 10.5 eV spectrum. Furthermore, there is a progressive loss of the high energy fragments (E_T>25 kcal/mol) as the ionization energy is decreased.

The P(E_T) distributions in Figure 7 contain valuable information on the contributions of each asymptotic channel to the dissociation. The fragments with translational energies greater than 17 kcal/mol must result from the lower energy S(^{3}P)

channel and translational energies near the thermodynamic limit (45 kcal/mol) correspond to CS fragments which have low internal energy. As expected, these fragments are not detected when the ionization energy is tuned below the CS ionization potential. At 10.5 eV only CS fragments containing 19 kcal/mol of internal energy will be efficiently ionized and this truncation of the $P(E_T)$ distribution is qualitatively observed. In the absence of the $S(^1D)$ channel the low translational energy region of the $P(E_T)$ would be unaffected at 10.5 eV. However, we observe a significant loss of the vibrational structure in the $P(E_T)$ at 11 eV which further suggests that this vibrational structure arises from the $S(^1D)$ channel. In addition, the observation of a significant fraction of low translational energy fragments at 10.5 eV proves that there is some contribution of $S(^3P)$ fragments in this energy range, corresponding to $S(^3P)$ formed in coincidence with highly excited CS fragments (v>10).

We have qualitatively modeled the dependence of the CS $P(E_T)$ on the photoionization energy shown in Figure 7. A detection function accounting for the finite width of the synchrotron radiation and including a linear onset function was used to describe the ionization probability as a function of energy above the threshold. The total $P(E_T)$ distribution was partitioned into two distributions corresponding to $S(^1D)$ and $S(^3P)$ channels. At each ionization energy, these were modified by the detection function described above and co-added, and the resulting simulation was compared to the experimental distributions. Shown in Figure 8 are two simulations which represent previous estimates of the $S(^1D)$ and $S(^3P)$ distributions. The panels to the left correspond to assigning the region of the total $P(E_T)$ less than 17 kcal/mol solely to the $S(^1D)$ channel. The series of panels to the right correspond to a decomposition resembling the LIF Doppler measurements of Waller and Hepburn and the assumed breakdown of Tzeng *et al.* The differences between the two sets of simulations are dramatic. Although the function used to model the ionization probability is approximate, the simulations provide qualitative information on the shapes and branching ratios of the two channels. The right panels successfully mimic the experimentally observed distributions shown in Figure 7 while the left panels do not. In addition, the $S(^1D)$ channel resulting from the partitioning on the right quantitatively fits the $P(E_T)$ in the lower panel of Figure 2, derived from the $S(^1D)$ TOF spectra. Based on an optimization of the partitioning we obtain a branching

ratio of 3.0±0.2 in good agreement with the value of 2.8±0.1 reported by Waller and Hepburn.[8]

D. Dissociation Dynamics

Absorption in CS_2 at 193 nm is due solely to a $^1B_2 \leftarrow X(^1\Sigma_g)$ transition with the transition dipole moment lying along the C-S bonds in the linear ground state molecule.[1] Several groups have determined anisotropy parameters for CS_2 dissociation at 193 nm. Bersohn and co-workers using a room temperature effusive beam observed no photofragment anisotropy and reported a lower limit to the lifetime of 0.6 ps.[12] A subsequent study by Waller and Hepburn[8] using a supersonic molecular beam source yielded anisotropy parameters for the asymptotic channels of $\beta(^3P) = 0.85 \pm 0.15$ and $\beta(^1D) = 0.99 \pm 0.15$. Based on these values and an assumed 20 K rotational temperature of the beam, the lifetime of the excited state was estimated to be 2 ps. Frey and Felder[15] were the first to observe a strong velocity-dependence to the anisotropy parameter, ranging from 1.3 for translational energies near the thermodynamic maximum to 0.4 at small translational energies when using neon as the carrier gas. The anisotropy parameters were found to decrease significantly when helium was used as a carrier gas over the entire range of translational energies. The authors suggested that the difference was due to the more efficient rotational cooling in the presence of neon as compared to helium. The apparent sensitivity of the measured anisotropy parameter to the expansion conditions suggests that the excited state lifetime is comparable to parent rotation. Frey and Felder estimated a lifetime of 1.5 ps based on their measured anisotropy parameters. Previous estimates of the dissociation time-scale determined from the product anisotropy, however, are at odds with time-resolved studies of the excited state lifetime. Baronavski and Owrutsky[28] observed a decreasing lifetime with increasing dissociation energy using ultrafast techniques to probe the excited CS_2 molecule. Although the study did not extend to 193 nm, the lifetime is expected to be significantly less than 1 ps. A more recent time-resolved experiment, including measurements at 194 nm, showed a similar trend in the excited state lifetime with increasing photon energy, yielding a lifetime of 180 ± 15 fs for 194 nm excitation.[29] As suggested by Frey and Felder, these time-resolved studies focus on the disappearance of the excited CS_2 and may not reflect the

time-scale associated with the formation of asymptotic products. The values of the anisotropy parameters determined in the present study are slightly lower than determined by Frey and Felder. We attribute this observed difference in the magnitude of the velocity-dependent anisotropy parameter primarily to a difference in expansion conditions of the molecular beams.

We have further characterized the velocity dependence of the anisotropy parameter reported previously by Frey and Felder,[15] who assumed that the observed velocity dependence of the anisotropy parameter was a result of two overlapping channels that were each described by a constant anisotropy parameter. The anisotropy parameter for the $S(^3P)$ channel was set to the observed value near the $S(^3P)$ thermodynamic threshold. The anisotropy parameter for the $S(^1D)$ channel was then adjusted to determine the correlated translational energy distribution for both channels through a fit to the velocity dependent anisotropy constrained to yield a $S(^3P)/S(^1D)$ branching ratio consistent with the value reported by Waller and Hepburn. The authors determined β=1.3 for the $S(^3P)$ channel and β=0.2 for the $S(^1D)$ channel. Since these values differ significantly, Frey and Felder proposed that different dissociation dynamics were associated with each product channel. Based on the anisotropy parameters, the $S(^3P)$ channel was thought to dissociate through a nearly linear geometry, while the $S(^1D)$ channel was thought to dissociate through a highly bent structure. Our results, however, indicate that *both* channels exhibit velocity-dependent anisotropy parameters that range from 0.6-0.7 ± 0.1 for translational energies near the thermodynamic maximum to 0.1 ± 0.1 at low translational energies, suggesting that the dissociation dynamics may be similar for both channels.

Mank, *et al.* have recently studied the predissociation dynamics of the $^1B_2$ state using VUV LIF detection to measure excitation spectra between 214 and 198 nm. Fits to the observed lineshapes have provided relative lifetimes and unimolecular reaction rates for both channels as a function of excitation wavelength. Two high-lying dissociative states ($^1\Pi$ and $^1\Delta$) are believed to cross the $^1B_2$ state.[30] In C_{2v} symmetry, both dissociative states split into states of $^1A_2$ and $^1B_2$ character. The $^1B_2$ components of each state form avoided crossings with the $^1\Sigma^+(^1B_2)$ state in nonlinear geometries. The $^1\Pi$ state crosses the $^1B_2$ state near the bottom of the well, resulting in a flat potential energy surface for dissociation in nonlinear geometries. Dissociation from K=1 states was observed to be

substantially faster than from K=0 states, suggesting Coriolis coupling of symmetric stretching and bending vibrations to the unbound asymmetric stretching coordinate. The absence of asymmetric vibrations in the excited state absorption spectrum also suggests that the molecule is unbound along this coordinate. Dissociation along such a flat potential should occur slowly, allowing the quasilinear molecule to bend prior to reaching the asymptotic CS-S distance. Significant bending will correspond to a decrease in the magnitude of the anisotropy parameter. The extent to which the molecule bends during the dissociation should be strongly correlated to the partitioning of energy into the asymmetric stretch coordinate. This should result in a range of anisotropy parameters that, for CS_2 dissociation, should decrease with decreasing translational energy, which is the observed experimental trend. Although much less information is available on the triplet surface that couples to the $^1B_2$ state to give S(^{3}P) products,[4] the velocity dependence of the anisotropy parameter is similar for each channel. Therefore, dissociation to the S(^{3}P) channel may proceed through a similar mechanism to that of the S(^{1}D) channel, implying that a curve crossing displaced along the reaction coordinate is present. A similar observation was made by Waller and Hepburn[8] based on their observation that the partitioning of the available energy into vibration was similar for each dissociation channel.

IV. CONCLUSIONS

The photodissociation of CS_2 at 193 nm was studied using the technique of photofragment translational spectroscopy with vacuum ultraviolet synchrotron radiation for product photoionization. The combination of state-selective ionization and high-resolution neutral time-of-flight has permitted a detailed view of the dissociation dynamics. The results also demonstrate the viability of measuring correlated scalar and vector distributions arising from photodissociation on the apparatus. Correlated CS vibrational state distributions, determined from the coincident S(^{1}D) fragments have been determined. The vibrational distribution peaks at v=3 and the simulation of the S(^{1}D) translational energy distribution is consistent with average CS rotational energies of 1-3

kcal/mole. Careful analysis of the photoionization dependence of the CS TOF spectra has provided the translational energy distribution for the CS + $S(^3P)$ channel. We have determined a $S(^3P)/S(^1D)$ branching ratio of 3.0±0.2 in good agreement with previous reports. The two dissociation channels exhibit velocity dependent anisotropy parameters that decrease with decreasing translational energy release, suggesting that the dissociation dynamics for both channels may be similar.

V. ACKNOWLEDGMENTS

The authors would like to acknowledge the technical assistance of Dr. David Blank. Work by SWN and WSM was partially supported by a Research Enhancement from Texas A&M University. The work by AGS, AR and OS was supported by the Director, Office of Energy Research, Office of Basic Energy Science, Chemical Sciences Division of the U. S. Department of Energy under contract No. DE-AC03-76SF00098. The experiments were conducted at the Advanced Light Source, Lawrence Berkeley National Laboratory which is supported by the same source.

Figure Captions:

Figure 1: Unpolarized TOF spectra for m/e 32 (S^+) photoproducts at a scattering angle of 10°, 40°, 60° and a photoionization energy of 15.0 eV. The circles are the experimental data and the solid lines are the forward convolution fits using the $P(E_T)$ in figure 2.

Figure 2: Top panel: The state-averaged $P(E_T)$ used to fit the TOF spectra in figures 1 and 3. The translational energies corresponding to CS vibrational state for each channel are indicated above the $P(E_T)$. The arrows represent the thermodynamic thresholds for each channel. Bottom panel: Simulated fit to the $S(^1D)$ $P(E_T)$ using Gaussian rotational energy distributions and the best fit vibrational branching ratios. The state-averaged $P(E_T)$ from the top panel (dashed line) is shown for comparison.

Figure 3: Unpolarized TOF spectra for m/e 44 (CS^+) at scattering angles of 30° and 40° and a photoionization energy of 15.0 eV. The circles are the experimental data and the solid lines are the forward convolution fits using the $P(E_T)$ shown in figure 2.

Figure 4: Top Panel: Polarized TOF spectra for m/e 32 (S^+) at 40° and a photoionization energy of 15.0 eV. The angle between the laser electric field vector and the detector axis, θ, is indicated. The fits are the result of using the $P(E_T)$ in figure 2 which has been coarsely divided into sections, each described by a single anisotropy parameter (see text for details). Bottom Panel: Integrated regions of the m/e 44 (CS^+) TOF spectra as a function of polarization angle taken at a source angle of 10°. The data and fits correspond to translational energy ranges 2.5-7.0 kcal/mol (solid circles) and 20-30 kcal/mol (open circles). The best fit anisotropy parameters are indicated.

Figure 5: Experimental TOF spectra for m/e 32 (S^+) at 40° and a photoionization energy of 13.0 eV (top panel) and 10.1 eV (bottom panel). The circles are the experimental data and the solid lines are the forward convolution fits to the data using the $P(E_T)$ in the upper panel of figure 2 for the 13 eV data and the $P(E_T)$ in the lower panel of figure 2 for the 10.1 eV data.

Figure 6: TOF spectra for m/e 44 (CS^+) photoproducts at a scattering angle of 30° and photoionization energies of 12.0, 11.0, and 10.5 eV. The circles are the experimental data and the forward convolution fits (solid lines) were obtained using the $P(E_T)$'s shown in figure 7.

Figure 7: The $P(E_T)$ distributions derived from fitting the TOF spectra shown in figure 6.

Figure 8: Simulations of the photoionization dependence of the CS $P(E_T)$ shown in figure 7. The top panels show the partitioning of the state-averaged $P(E_T)$ (solid line) into contributions from the $S(^1D)$ and $S(^3P)$ channels (dashed lines). The lower panels are the $P(E_T)$ distributions resulting from decreasing the photoionization energy in accordance with the model described in the text.

References

[1] A. E. Douglas and I. Zanon, *Can. J. Phys.* **42**, 627 (1964).

[2] R. J. Hemley, D. G. Leopold, J. L. Roebber, and V. Vaida, *J. Chem. Phys.*, **79**, 5219 (1983).

[3] J. L. Roebber and V. Vaida, *J. Chem. Phys.* **83**, 2748 (1985).

[4] A. Mank, C. Starrs, M. N. Jego, and J. W. Hepburn, *J. Chem. Phys.* **104**, 3609 (1996).

[5] M. F. Arendt and L. J. Butler, *J. Chem. Phys.* **109**, 7835 (1998).

[6] M. deSorgo, A. J. Yarwood, O. P. Strausz, and H. E. Gunning, *Can. J. Chem.* **43**, 1886 (1965).

[7] M. C. Addison, R. J. Donovan, and C. Fotakis, *Chem. Phys. Lett.* **74**, 58 (1980).

[8] I. M. Waller and J. W. Hepburn, *J. Chem. Phys.* **87**, 3261 (1987).

[9] J. E. Butler, W. S. Drozdoski, and J. R. McDonald, *Chem. Phys.* **50**, 413 (1980).

[10] V. R. McCrary, R. Lu, D. Zakheim, J. A. Russell, J. B. Halpern, and W. M. Jackson, *J. Chem. Phys.* **83**, 3481 (1985).

[11] H. Kanamori and E. Hirota, *J. Chem. Phys.* **86**. 3901 (1986).

[12] S. Yang, A. Freedman, M. Kawasaki, and R. Bersohn, *J. Chem. Phys.* **192**, 4048 (1980).

[13] M. D. Barry, N. P. Johnson, and P. A. Gorry *J. Phys. E* **19**, 815 (1986).

[14] W.-B. Tzeng, H.-M. Yin, W. Y. Leung, J. Y. Luo, S. Nourbakhsh, G. D. Flesch, and C. Y. Ng., *J. Chem. Phys.* **88**, 1658 (1988).

[15] J. G. Frey and P. Felder, *Chem. Phys.* **202**, 397 (1996).

[16] X. Yang, J. Lin, Y. T. Lee, D. A. Blank, A. G. Suits, and A. M. Wodtke, *Rev. Sci. Instrum.* **68**, 3317 (1997).

[17] Y. T. Lee, J. D. McDonald, P. R. LeBreton, and D. R. Herschback, *Rev. Sci. Instrum.* **40**, 1402 (1969); N. R. Daly, *ibid* **31**, 264 (1960).

[18] M. Koike, P. A. Heimann, A. H. Kung, T. Namioka, R. DiGennaro, B. Gee, N. Yu, Nuclear Instruments and Methods in Physics Research 347, 282 (1994).

P. A. Heimann, M. Koike, C. W. Hsu, M. Evans, C. Y. Ng, D. Blank, X. M. Yang, C. Flaim, A. G. Suits, Y. T. Lee, SPIE Proceedings 2865 (1996).

[19] A. G. Suits, P. Heimann, X. Yang, M. Evans, C. Hsu, K. Lu, and Y. T. Lee, *Rev. Sci. Instrum.* **66**, 4841 (1995).

[20] X. Zhao, Ph.D. Thesis, University of California, Berkeley (1989).

[21] H. Okabe, *J. Chem. Phys.* **56**, 4381 (1972).

[22] V. H. Dibeler and J. A. Walker, *J. Opt. Soc. Am.* **57**, 1007 (1967).

[23] S. Dunlavey, J. Dyke, N. Fayad, N. Jonathan, and A. Morris, *Mol. Phys.* **38**, 729 (1979).

[24] V. R. McCrary, R. Lu, D. Zakheim, J. A. Russell, J. B. Halpern, and W. M. Jackson, *J. Chem. Phys.* **83**, 3481 (1985).

[25] D. A. Blank, S. W. North, D. Stranges, A. G. Suits, and Y. T. Lee, *J. Chem. Phys.* **106**, 539 (1997).

[26] D. A. Blank, W. Sun, A. G. Suits, Y. T. Lee, S. W. North, and G. E. Hall, *J. Chem. Phys.* **108**, 5414 (1998).

[27] J. Coppens and J. Drowat, *Chem. Phys. Lett.* **243**, 108 (1995).

[28] A. P. Baronavski and J. C. Owrutsky, *Chem. Phys. Lett.* **221**, 419 (1994).

[29] P. Farmanara, V. Stert, and W. Radloff, *J. Chem. Phys.* **111**, 5338 (1999).

[30] M. N. Jego, Ph. D. Thesis, Université Paris XI, 1993.

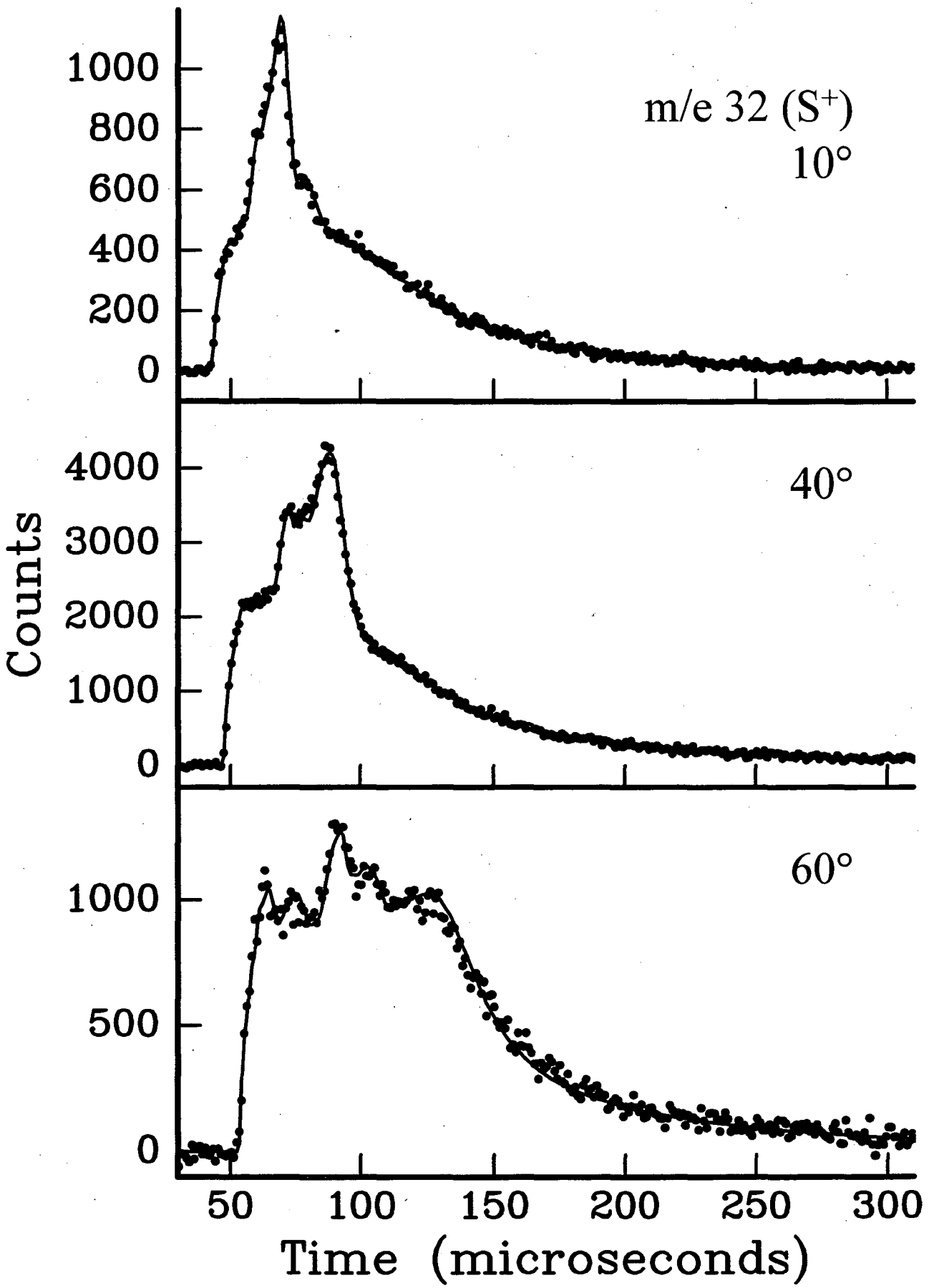
m/e 32 (S^+)
10°
40°
60°
Counts
1000
800
600
400
200
0
4000
3000
2000
1000
0
1000
500
0
50
100
150
200
250
300
Time (microseconds)

Fig 1

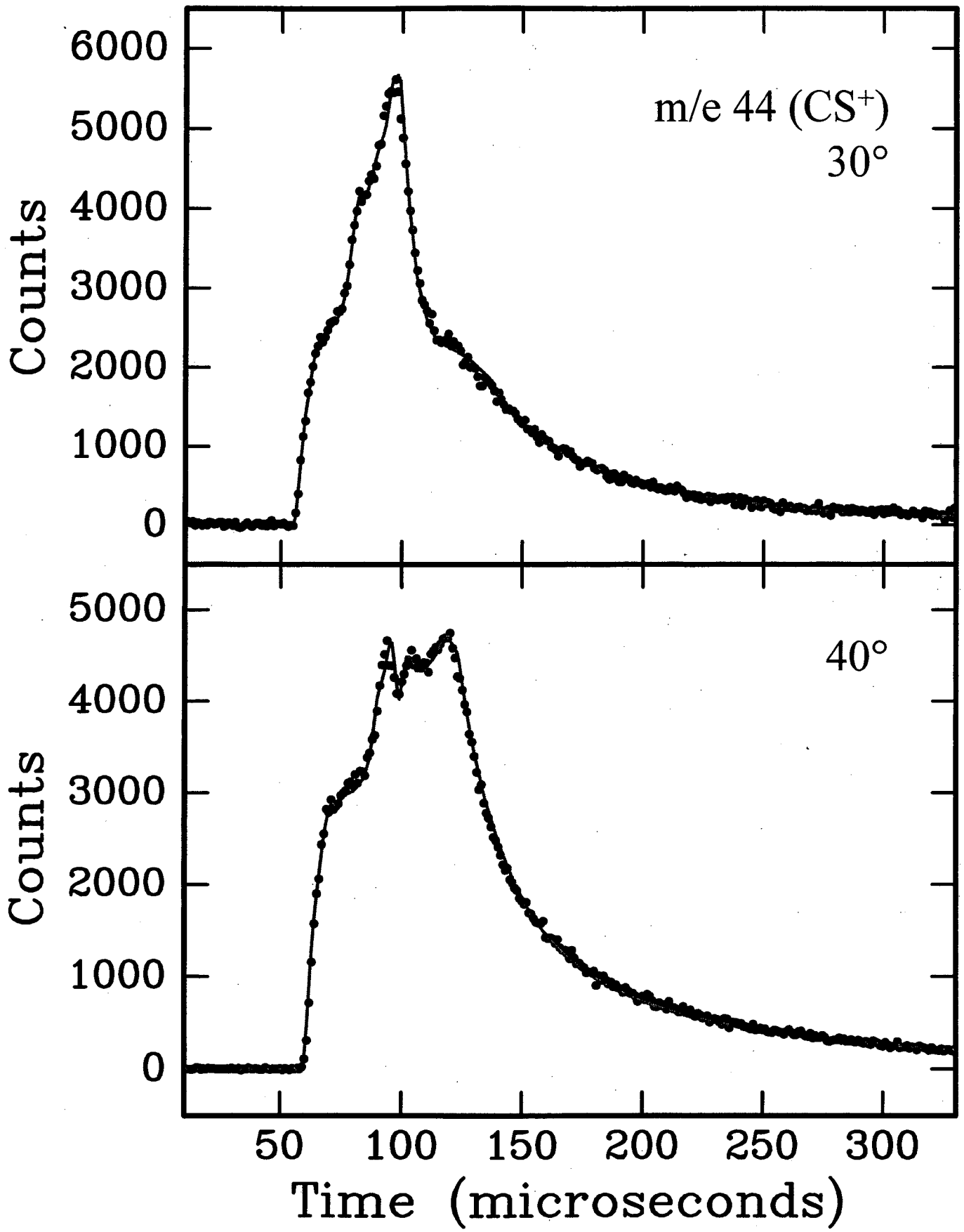
m/e 44 (CS+)
30°
40°
Counts
Counts
6000
5000
4000
3000
2000
1000
0
5000
4000
3000
2000
1000
0
50
100
150
200
250
300
Time (microseconds)

Fig 2

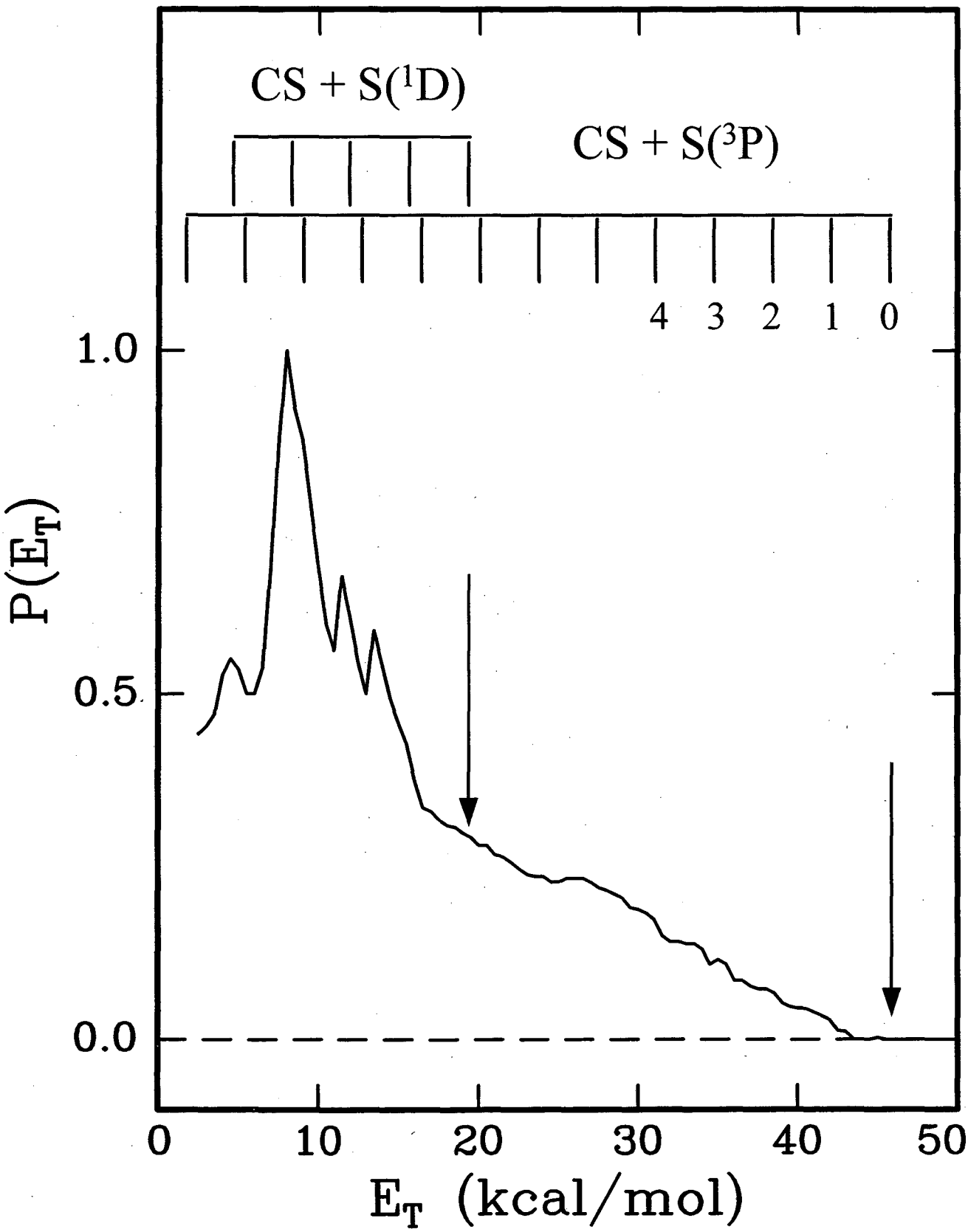

Fig 3

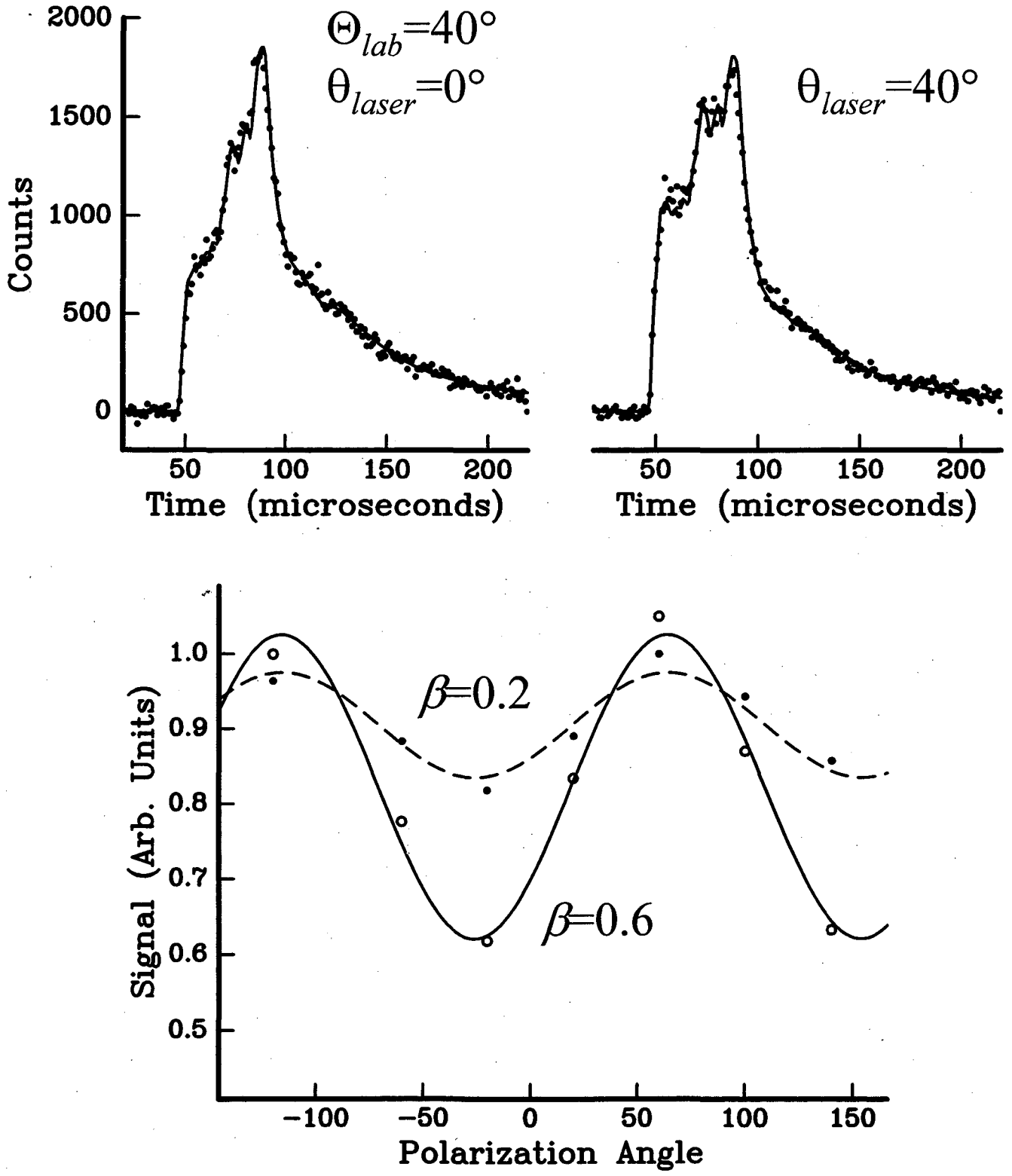
Θ_{lab}=40°
θ_{laser}=0°
Counts
2000
1500
1000
500
0
50
100
150
200
Time (microseconds)
θ_{laser}=40°
50
100
150
200
Time (microseconds)
Signal (Arb. Units)
1.0
0.9
0.8
0.7
0.6
0.5
β=0.2
β=0.6
−100
−50
0
50
100
150
Polarization Angle

Fig. 4

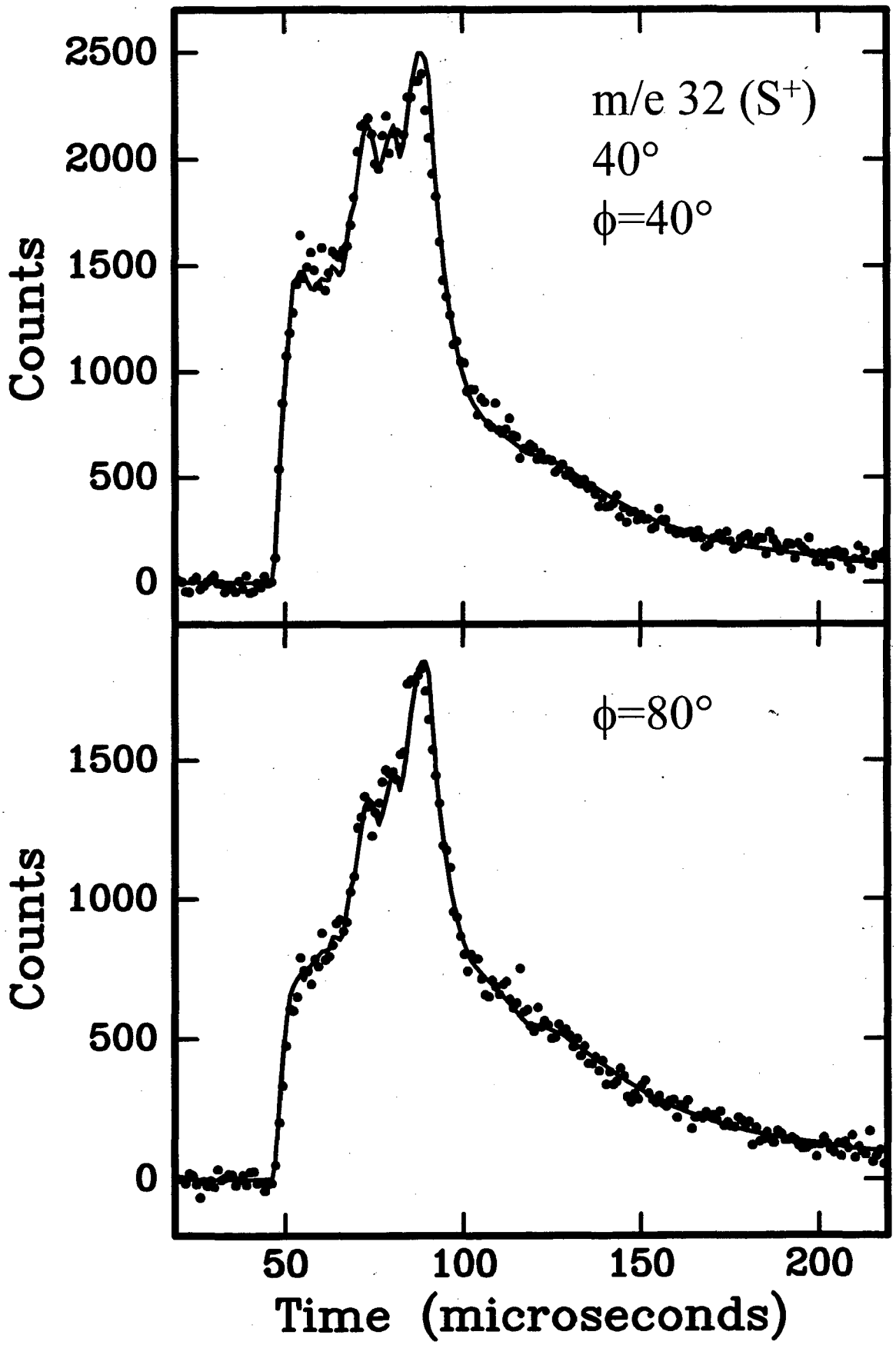
m/e 32 (S+)
40°
ϕ=40°
ϕ=80°
Counts
Counts
2500
2000
1500
1000
500
0
1500
1000
500
0
50
100
150
200
Time (microseconds)

Fig 5

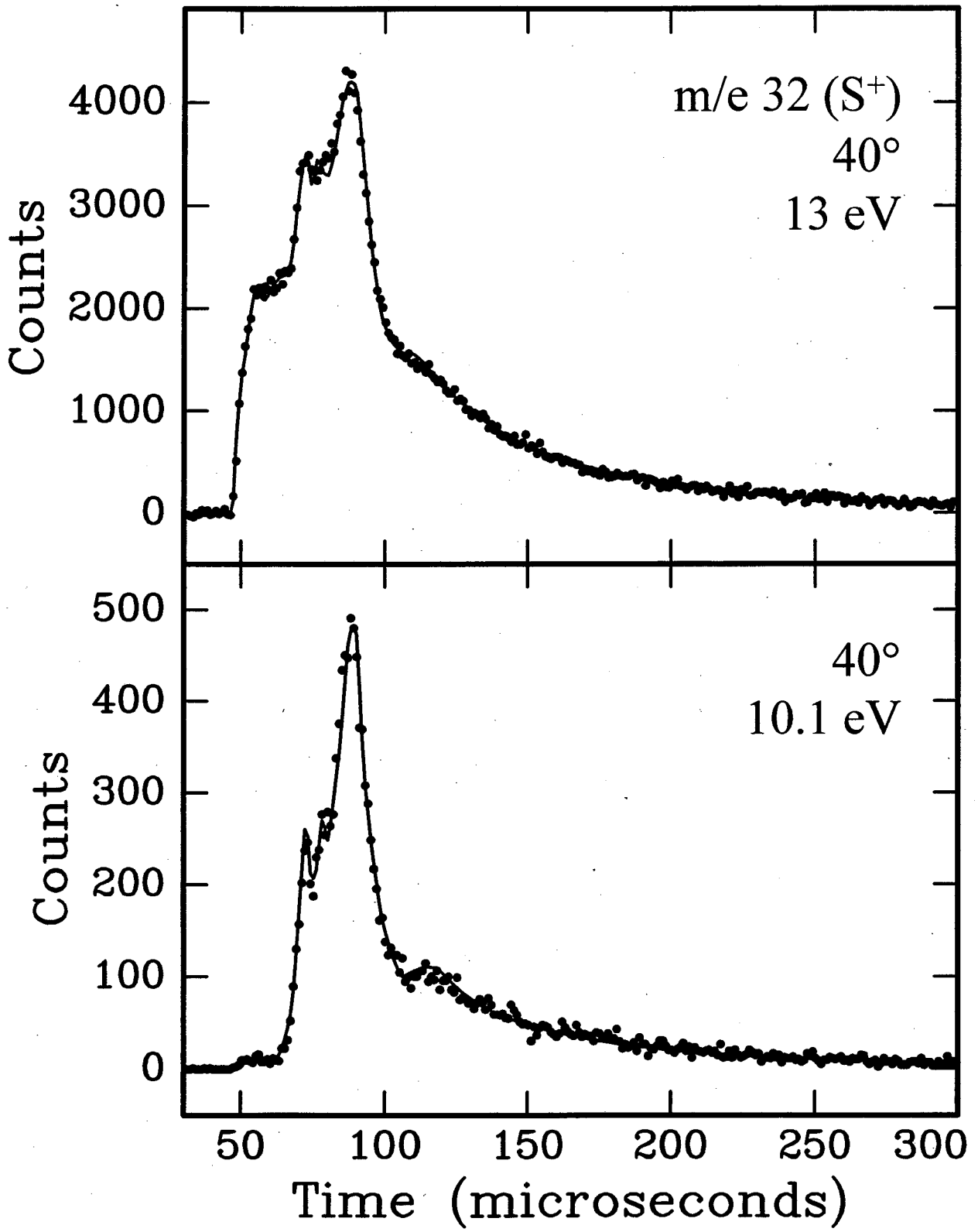
m/e 32 (S+)
40°
13 eV
Counts
4000
3000
2000
1000
0
40°
10.1 eV
Counts
500
400
300
200
100
0
50
100
150
200
250
300
Time (microseconds)

Fig. 6

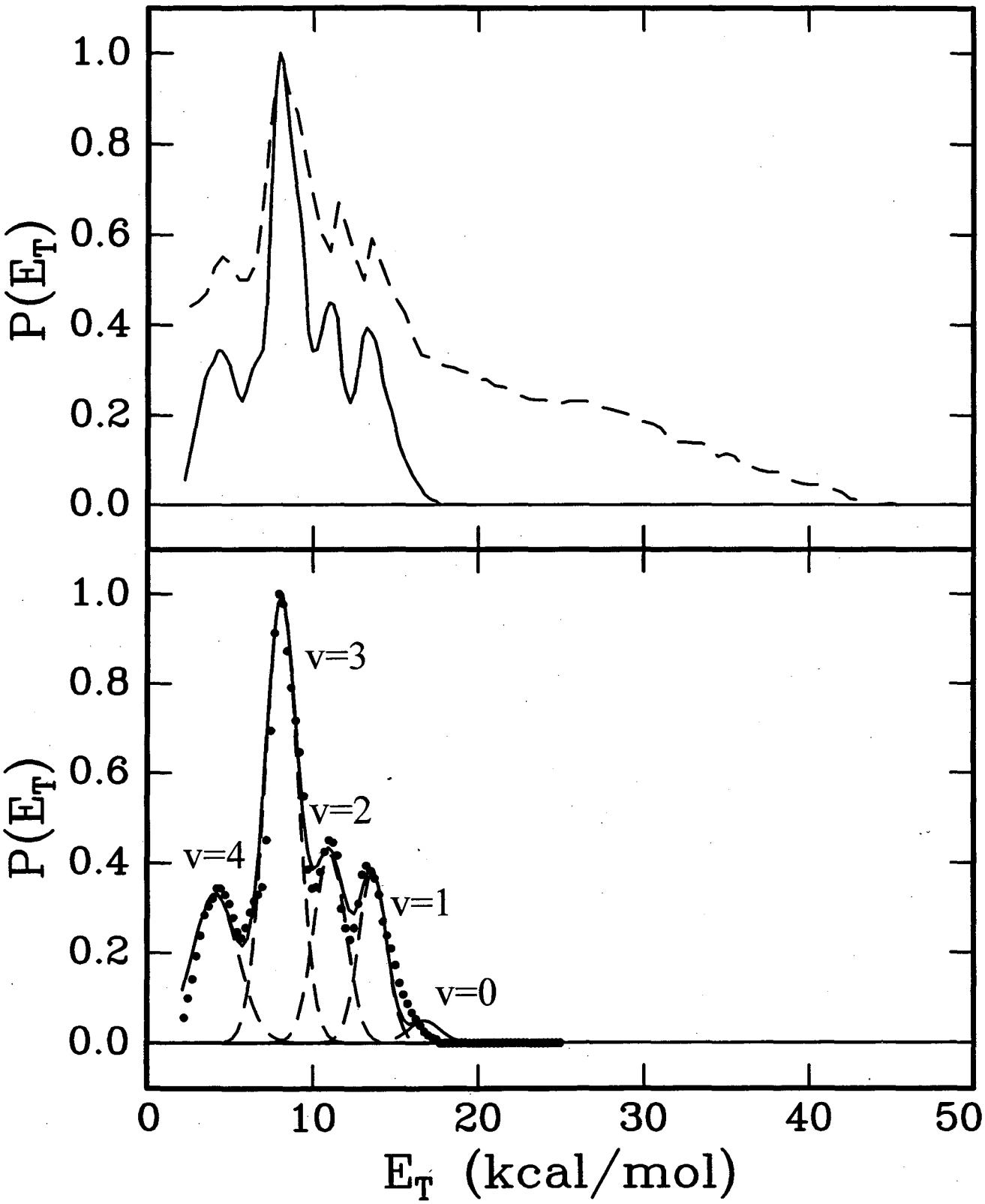

Fig 7

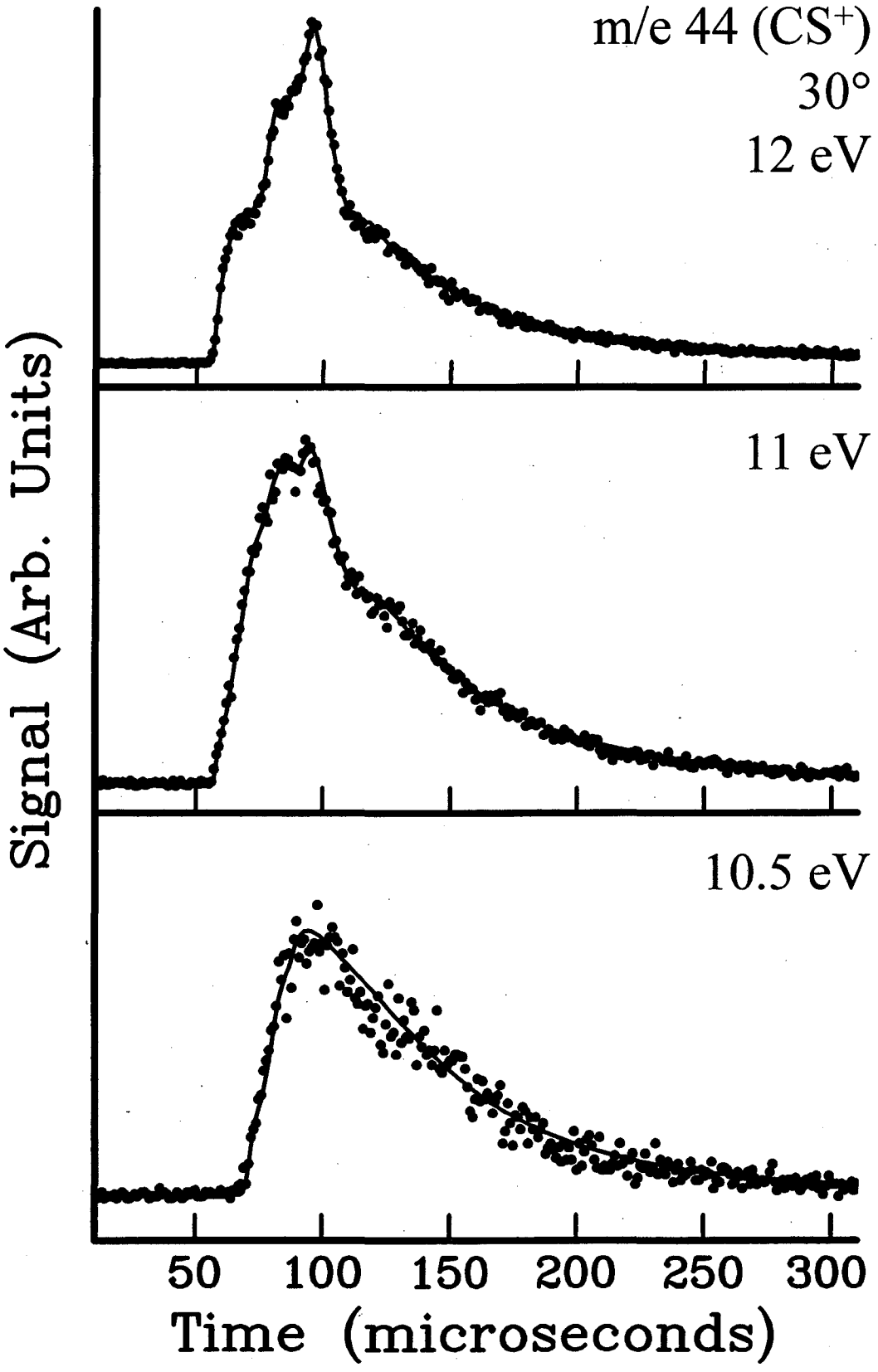
m/e 44 (CS^+)
30°
12 eV
11 eV
10.5 eV
Signal (Arb. Units)
50
100
150
200
250
300
Time (microseconds)

Fig 8

ERNEST ORLANDO LAWRENCE BERKELEY NATIONAL LABORATORY
ONE CYCLOTRON ROAD | BERKELEY, CALIFORNIA 94720

Prepared for the U.S. Department of Energy under Contract No. DE-AC03-76SF00098